Coupled Finite Element and Multibody Systems Dynamics Modelling to Investigate the Bridge Approach Problem

A. I. El-Ghandour and C. D. Foster *

Department of Civil and Materials Engineering, University of Illinois at Chicago, Chicago, IL, USA,
e-mail: fosterc@uic.edu

Acknowledgements

This project was supported by the National University Rail (NURail) Center - a US DOT OST-R University Transportation Center.

Abstract: Rail has been one of the most commonly used modes of transportation for both people and cargo due to its advantages in economy, safety, and comfort. The Finite Element Method (FEM) has been used broadly for more than three decades to model the different components of the railroad system such as rails, sleepers (cross ties), and substructure and have been used to investigate variety of problems associated with rail mechanics. Different Multibody Systems Dynamics (MBS) software programs have also been developed to investigate the dynamic performance and contact behaviour between the rails and the wheels and to determine the contact forces. In this work, a full 3D model that couples both FEM and MBS has been used to study the railroad system. The main focus of this study is to model the bridge approach problem under dynamic load. The bridge approach problem arises from the sudden change in the foundation's stiffness under the rails at the bridge entry and exit, leading to high levels of stress and settlement that can also cause further problems over time. The effect of using a concrete slab at the bridge entry is also investigated in this study, using

*Corresponding Author. Email: fosterc@uic.edu, Tel.: +1-312-996-8086, Fax:+1-312-996-2426.

two slab designs: rectangular and inclined. The results show the effectiveness of the 3D model and slab implementation on the forces and the vertical deformation, especially the inclined slab that applies a gradual change in the stiffness rather than a sudden change.

Keywords and phrases: Train-track-soil-model, Finite element method, Multibody dynamics, Modal analysis, Bridge approach.

1. Introduction

Numerical modelling of train dynamics now has a wide role in researching many issues in the industry. To accurately evaluate mechanical issues in the ballast or subgrade, however, a detailed model of this substructure is needed. Most researchers modelling rail dynamics have assumed in their work rigid substructures, and therefore the models did not include the deformability of the soil layers, even if they included rail flexibility. Some researchers, however, included the effect of the substructure by simplifying it and modelling it as spring-dampers elements. Xiao et al. [1] and Xiao et al. [2] studied the problem of track support failure. The substructure was modelled in both work using spring-damper elements. The vehicles' dynamic response was investigated in [1] on linear track, while in [2], the vehicle derailment was investigated over a curved track with lack of track support in both models at certain locations.

A few researchers have created a full continuum model using the finite element method to model the different layers of the substructure. Chebli et al. [3] created a FE model to investigate the in-situ measurement and the dynamic responses of high-speed trains. FEM was also used by Kumaran et al. [4] to model the different components of the railroad system (rails, sleepers, ballast and subballast) to study the dynamic response of prestressed concrete sleepers and the interaction between the wheels and the rails. Koskinen [5] used FEM to study the substructure effect on the rails, by modelling the bridge, railway and soil. In finite elements, the ballast is usually modelled, as described above, using springs or solid elements. Another method used to model the ballast is the discrete element method (DEM). The discrete element method models each particle of ballast or soil (sometimes as aggregates) separately, using simplified contact formulations to describe their interaction. DEM has been used to study the case of the uneven ballast set-

tlement and the displacement of the rail associated with it by Tutumluer [6]. Tutumluer focused on the properties of the ballast such as gradation, aggregate type, and angularity. The study showed that the level of plastic deformation is increased with increasing load. It is important to mention here that the discrete element method, while it can model each ballast particle, it is computationally expensive and has not yet been integrated with a full vehicle model.

Wu et al. [7] created a 3D model to investigate the vehicle-track-bridge interaction. The model simplified the substructure as springs and dampers. The results showed the effect of the lateral and torsional vibration of the bridge on selecting the moving speed. Two indices were created to select the train speed in the case of two trains moving in opposite directions on the same track.

Multibody systems have also been widely used in the rail industry ([8, 9], among many others). With the high level of usage of both FEM and MBS in the rail industry over the last few decades, coupling the techniques in the same simulation has proven very valuable for many problems. The benefit of coupling both FEM and MBS is the ability to profit from the advantages of each technique. For example, using the FEM is more efficient for simulating the substructure and the sleepers' elasticity; however, using the MBS is more efficient for modelling the contact between the wheel and the rail. In contrast to many studies in the literature, where the researchers either used FEM or MBS to study a specific problem, this coupled model imparts the ability to investigate different scenarios of different components of the rail system with greater accuracy and efficiency.

A number of researchers have worked on coupling both FEM and MBS to create more accurate and sophisticated models to investigate more complex scenarios. Galvin et al. [10] built a full 3D model to dynamically analyse the interaction among the trains, track, and substructure. The vehicles were modelled using MBS while FEM was used to model the track. The soil was modelled using the boundary element method by building a homogenous half-space model. Tanabe et al. [11] also coupled MBS and FEM in their work. They focused on the dynamic interaction between the train and the substructure in the case of earthquakes. They also studied the behaviour after derailment. Using independent dynamic integration algorithms, Ambrósio et al. [12] coupled FEM and MBS to investigate a pantograph-catenary inter-

action. FEM was used to model the catenary and MBS used to model the pantograph. El-Ghandour et al. [13] studied the effects of substructure stiffness on wheel-rail dynamics, including the problem of unsupported sleepers.

While many researchers have been attracted to study the above-mentioned problems, bridge approaches and other transitions have attracted particular attention due to the impact to the rail system and related costs. The difference in the stiffness between bridge abutments and the surrounding soil causes many problems in the railroad industry. The sudden stiffness changes can cause increased stress, which consequently increases settlement at the transition. These differential settlements create a rapid change in the rail height at the bridge approach, which leads to higher forces and increased wear in the track and the wheels. This wear, in turn, creates a need for extra maintenance cost. The main causes of this problem are poor soil compaction, natural settlement under the embankment, and excessive traffic loads. See Briaud et al. [14] for more detailed discussion of these issues.

Several solutions have proposed to mitigate the settlement around transitions. Using a finite element model, Monley and Wu [15] simulated the effect of the geogrid tensile reinforcement that is placed in the approach fill before the abutment. They also studied the effect of including a collapsible inclusion between the tensile reinforcement and the abutments walls. The latter case showed better results compared to the case of only tensile reinforcement due to the effect of inclusion on the lateral load reduction.

Helwany et al. [16] used FEM to study the performance of a geosynthetic-reinforced soil (GRS) bridge abutment and its effect on the foundation soil settlement. The study also included the effect of the soil density combined with the GRS bridge abutment. Their results showed that the GRS bridge abutment performed nicely with dense soil. On the contrary, the case of loose soil showed large level of abutment displacement.

Li and Davis [17] conducted another study, in which the field tests were performed on four different bridge approaches in order to determine the causes and the remedies of the track geometry degradation and its link to the sudden change in the stiffness at the bridge approach. They studied the influence of the stiffnesses of the different layer and found that the ballast and subballast have more impact on the stiffness issue than the subgrade layer. Adding a rubber mat underneath the concrete ties to improve the damping was recommended as well.

Dahlberg [18] used finite elements to study the degradation of the rail due to the track stiffness variation. Dahlberg's FE model included a transient section in the rail where the stiffness is increased gradually between the two zones with significant difference in the track stiffness values. Also, he tested a case where an under-sleeper pad (elastomeric product) was used as another method to provide a desired stiffness transition zone in the middle of the track. He obtained similar results by gradually increasing the ballast stiffness under each sleeper from the low stiffness zone to the high stiff zone. An optimisation analysis was performed to obtain the suitable stiffnesses for each transition zones in the different cases.

Zhang et al. [19] performed a comparison analysis between the conventional geogrid-reinforced and pile-supported embankments, as well as a combined fixed-geogrid-reinforced and pile-supported embankment. The effectiveness of both techniques on the bridge approach settlement was assessed using numerical analysis, the fixed-geogrid-reinforced technique showed better results on both settlement and lateral displacement.

Another solution that is common between both highways and railroad bridge approach problem is the implementation of slab in the substructure before the bridge. Slabs have been used in highways since the 1970s, and the wedge-shaped transition zone was implemented by the Japanese National Railways in railroad bridges as a solution for the variation of stiffness problem [20]. The purpose of this slab, which can be flat or wedge-shaped, is to increase the substructure stiffness in the low stiffness zone before the bridge to provide smoother transition in the stiffness value at the bridge approach. Detailed studies about the slab design and implementation are performed in [21] and [22].

The purpose of this study is to create a detailed bridge model that contains the main components of the railroad system by coupling both FEM and MBS codes in the time domain to study the bridge approach problem where the stiffness variation on the entrance and the exit affect the train performance. The wheel-rail contact is modelled using MBS. The FEM model includes the rails, fasteners, sleepers, and substructure as deformable bodies. The continuum finite element model allows us to provide details geometry of the substructure in a way that captures the stiffness change across the transition. We will use this model to evaluate the effectiveness of two different approach slab designs in reducing the stress at the transitions.

The analysis in this work is performed using the modal frequencies extracted from the FE model instead of the nodal degrees of freedom, and uses the Floating Frame of Reference (FFR) formulation to obtain the elastic response of the system. After the multibody dynamics analysis is run, we reconstruct the full solution in the substructure model. To our knowledge, this is the first time that such a coupled formulation has been applied to the problem of bridge approaches. The rest of this paper is structured as follows: in Section 2, the FE model is explained in detail. The main formulations of the MBS analysis and the contact force equations are also explained. Section 3 includes the numerical results of the work, followed by the conclusions in Section 4.

2. Modelling

In this section, we detail the coupled FE and MBS model for the bridge approach problem. Here, finite element modelling is used to model the different components of the problem, including rails, sleepers, substructure and the bridge. Using beam, solid and spring elements, a full 3D model is created. Both dynamic analysis and wheel-rail contact forces are modelled using a MBS code. The finite element model is described in the following subsection, including material properties and dimensions. The subsequent subsection discusses the MBS formulations.

2.1. FE Model

In this work, the commercial FE software ANSYS has been used to model the components of the bridge system. Figure 1 shows the bridge full model.

Beam elements are used to model rails, sleepers and concrete beams, while solid elements have been used for the rest: substructure layers (ballast, sub-ballast, and subgrade), bridge deck, and abutments. The fasteners between the sleepers and the rails are modelled using spring-damper elements. Table 1 shows the material properties of the different materials used in the bridge model and also the main dimensions of the model.

Two approach slabs were considered, one rectangular and one inclined. The rectangular slab is 0.25 m thick, while the inclined slab varies 0.25 to 1.25 m

TABLE 1
Finite element model materials properties and dimensions.

Description	Symbol	Value	Unit
Rail stiffness	E_r	210×10^9	N/m^2
Rail density	ρ_r	7700	kg/m^3
Rail Poisson's ratio	ϵ_r	0.3	
Sleeper stiffness	E_s	64×10^9	N/m^2
Sleeper density	ρ_s	2750	kg/m^3
Sleeper Poisson's ratio	ϵ_s	0.25	
Concrete beam stiffness	E_{bm}	31×10^9	N/m^2
Concrete beam density	ρ_{bm}	2500	kg/m^3
Concrete beam Poisson's ratio	ϵ_{bm}	0.2	
Deck stiffness	E_d	31×10^6	N/m^2
Deck density	ρ_d	2500	kg/m^3
Deck Poisson's ratio	ϵ_d	0.25	
Ballast stiffness	E_b	260×10^6	N/m^2
Ballast density	ρ_b	1300	kg/m^3
Ballast Poisson's ratio	ϵ_b	0.3	
Sub-ballast stiffness	E_{sb}	200×10^6	N/m^2
Sub-ballast density	ρ_{sb}	1850	kg/m^3
Sub-ballast Poisson's ratio	ϵ_{sb}	0.35	
Sub-grade stiffness	E_{sg}	200×10^6	N/m^2
Sub-grade density	ρ_{sg}	1850	kg/m^3
Sub-grade Poisson's ratio	ϵ_{sg}	0.3	
Abutment stiffness	E_a	20×10^9	N/m^2
Abutment density	ρ_a	2500	kg/m^3
Abutment Poisson's ratio	ϵ_a	0.3	
Slab stiffness	E_{sl}	31×10^9	N/m^2
Slab density	ρ_{sl}	2500	kg/m^3
Slab Poisson's ratio	ϵ_{sl}	0.25	
Fastener stiffness	K_f	70×10^8	N/m
Rail length	L_r	30	m
Gauge length	G	1.5113	m
Rail cross section area	A_r	64.5×10^{-4}	m^2
Rail second moment of inertia	$I_{R_{yy}}$	2010×10^{-8}	m^4
Rail second moment of inertia	$I_{R_{zz}}$	326×10^{-8}	m^4
Concrete beam length	b_l	12	m
Concrete beam width	b_w	0.3	m
Concrete beam depth	b_d	0.75	m
Sleeper Length	L_s	2.6	m
Gap between sleepers	g_s	0.6	m
Sleeper cross section area	A_s	513.8×10^{-4}	m^2
Sleeper second moment of inertia	$I_{S_{yy}}$	25735×10^{-8}	m^4
Sleeper second moment of inertia	$I_{S_{zz}}$	18907×10^{-8}	m^4
Ballast Depth	B_d	0.6	m
Sub-ballast Depth	SB_d	0.25	m
Sub-grade Depth	SG_d	8.5	m

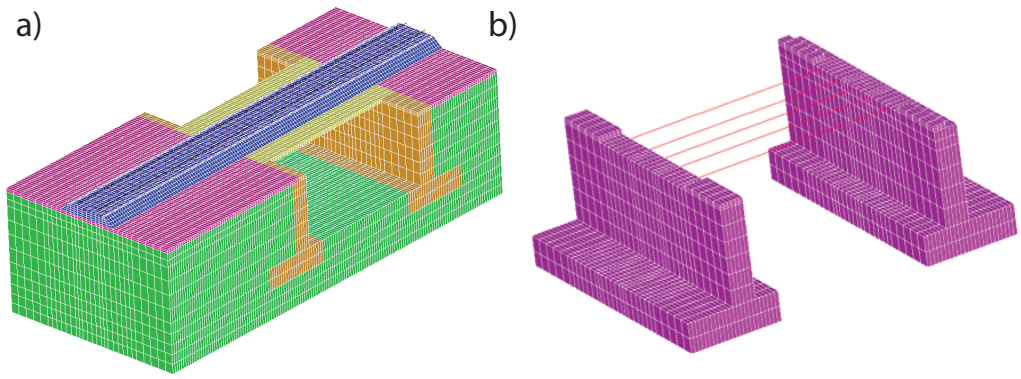

Fig 1: a) Full 3D Finite Element Model of the bridge approach. (Blue: Ballast, Red: Subballast, Green: Subgrade, Yellow: Deck, Orange: Abutment). b) Cutaway showing the beams under the bridge.

thick. Both slabs are 6 m long and 2.6 m wide. from The slab geometries are shown in Figure 2. Additionally, a case with no approach slab was considered.

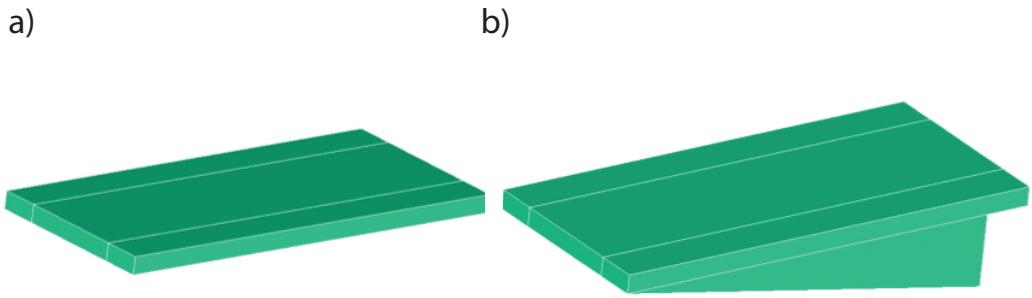

Fig 2: Geometry of two proposed approach slabs: a) rectangular slab, and b) inclined slab

2.2. Boundary conditions

The rail is modelled using beam elements with its beginning and end nodes fully constrained. The ballast, subballast, subgrade, deck, and abutments are modelled using solid elements. The bottom face of the model, sub-grade, is fixed in all directions, while the nodes that fall on any of the four sides are constrained in the direction perpendicular on that surface that contain these nodes. The common nodes between the sleepers and ballast are constrained for the rotational degrees of freedom as the solid elements only have translational degrees of freedom while the beam elements have six degrees of freedom, three translational and three rotational. Also, the rotational degrees of freedom of the common nodes between the spring elements and the beam elements of the rail were constrained.

2.3. Coupling Finite element with Multibody Systems

As we are trying to benefit from both FEM and MBS, we need to couple them in an efficient way to reduce the time with out losing the accuracy. We start by applying modal analysis on the FE model and extract the mode shapes and eigenvalues. We then select a certain number of the mode shapes that covers the main frequencies and different modes of the system. Once the modes have been selected, the nodal elimination process is applied. The multibody code only requires the modal information for nodes that are involved in the contact with the vehicle or receive external forces. Hence, we retain the nodes under external forces and contact, which in our case are the nodes of the rails. We then provide the MBS code with the part of the modal information (mode shapes, frequencies and damping) associated with the selected nodes. This approach allows us to build a very complex model with large number of elements, but perform the dynamic analysis based on the selected modes and nodes and achieve significant reduction in the simulation time. This process is described in more detail in [13]. Using a Dell Inc. PowerEdge T420 machine with Intel Xeon CPU E5-2450 v2 2.5 GHz processor, the simulation times for the modal analysis and the dynamic analysis (interaction between the wheel and the rail) are roughly 25 and 20 min respectively. The memory consumed are 3546 and 250 MB for the modal and the dynamic analysis respectively. These values are for 250 mode shapes.

2.4. Floating Frame of Reference and Equations of Motion

Multibody systems have been coupled with finite elements in this work. The rails were modelled in the MBS code as flexible body using Floating Frame of Reference (FFR) formulation which is introduced into the equations of motion. FFR is used here to benefit from the component-mode representation of a Finite Element model.

$$\mathbf{r}^r = \mathbf{R}^r + \mathbf{A}^r(\overline{\mathbf{R}}^{rp} + \mathbf{A}^{rp}\overline{\overline{\mathbf{U}}}^{rp}) \tag{2.1}$$

where $\mathbf{r}^r$ is an arbitrary point position on the surface of the rail, $\mathbf{R}^r$ is the location of the track coordinate system location with respect to the global coordinate system, $\overline{\mathbf{R}}^{rp}$ is the rail profile coordinate system location with respect to the track coordinate system, $\mathbf{A}^{rp}$ is the profile coordinate system orientation with respect to the track coordinate system, and $\overline{\overline{\mathbf{U}}}^{rp}$ is a point on the rail surface in the profile frame.

In this investigation, the FE model was coupled with MBS to use its contact calculations to simulate the contact between the wheel and the rail. Many techniques are available in the literature for this purpose, such as the linear superposition used by Meli and Pugi [23]to approximate the contact in faster way. In this study, the 3D non-conformal approach contact scheme presented in [24] is used to predict the contact point location. This technique is called the Elastic Contact Formulation for Algebraic Equations (ECFA) approach. In this approach, the contact surface is presented using the surface parameters, which are two non-generalised coordinates. This allows the contact point location to be defined by two independent coordinates only.

For the governing equations of motion, the augmented form of the equations of motion used in this study is given below. This form was presented in [25].

$$\begin{bmatrix} \mathbf{m}_{rr} & \mathbf{m}_{rf} \\ \mathbf{m}_{fr} & \mathbf{m}_{ff} \end{bmatrix} \begin{bmatrix} \ddot{\mathbf{q}}_r \\ \ddot{\mathbf{q}}_f \end{bmatrix} = \begin{bmatrix} (\mathbf{Q}_e)_r \\ (\mathbf{Q}_e)_f \end{bmatrix} + \begin{bmatrix} (\mathbf{Q}_v)_r \\ (\mathbf{Q}_v)_f \end{bmatrix} - \begin{bmatrix} \mathbf{C}_{\mathbf{q}_r}^T \\ \mathbf{C}_{\mathbf{q}_f}^T \end{bmatrix} \lambda - \begin{bmatrix} \mathbf{0} \\ \mathbf{K}_{ff}\mathbf{q}_f \end{bmatrix} \tag{2.2}$$

where the inertia matrices that are related to the reference coordinates and the elastic coordinates are represented by $\mathbf{m}_{rr}$ and $\mathbf{m}_{ff}$ respectively, while the inertia matrices that are related to dynamic coupling of both elastic and reference coordinates are presented by $\mathbf{m}_{rf}$ and $\mathbf{m}_{fr}$. The generalised rigid-body coordinate vector is presented by $\mathbf{q}_r$, the FFR elastic modal coordinate vector which describe the flexibility of both the track and the substructure is represented by $\mathbf{q}_f$, the generalised external force vector associated with the rigid coordinates is presented by $(\mathbf{Q}_e)_r$ while the generalised external force vector associated with the elastic coordinates is presented by $(\mathbf{Q}_e)_f$, the quadratic velocity inertia force vector that is related to the rigid coordinates is presented by $(\mathbf{Q}_v)_r$ while the quadratic velocity inertia force vector that is related to the elastic coordinates is presented by $(\mathbf{Q}_v)_f$, the constraint Jacobian matrix that is related to the rigid coordinates is represented by $\mathbf{C}_{\mathbf{q}_r}$ while the constraint Jacobian matrix that is related to the elastic coordinates is represented by $\mathbf{C}_{\mathbf{q}_f}$, the Lagrange multipliers vector is represented by $\boldsymbol{\lambda}$, and the matrix of the track stiffness is represented by $\mathbf{K}_{ff}$. These equations are solved for the generalised accelerations and the Lagrange multipliers using the explicit Adams-Bashforth predictor-corrector numerical integration scheme. The independent coordinates and velocities are determined. Further details can be found in [25, 26, 27].

In this investigation, the MBS code SAMS/2000 [28] was used to perform the dynamic analysis. This dynamic analysis was performed on the wheelset shown in Figure (3) with its mechanical information are listed in Table (2). The wheelset was used here to investigate the methodology presented in this work. While adequate for testing the numerical method, it misses some of the motions of a real train, including pitch movement. A longer train model will be the subject of future investigations.

The wheelset is running with speed of 30m/s over a straight track in all the simulations.

2.5. Reconstruction of Data

The dynamic analysis of the MBS will provide us with the modal displacement and modal velocity for the rails nodes. Therefore, it is important to reconstruct the data for the whole system based on these outputs and the

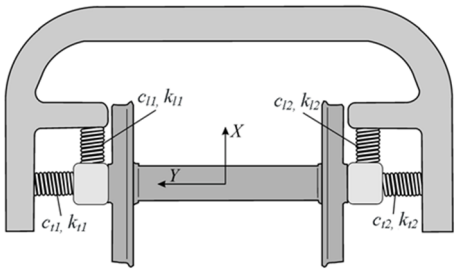

Fig 3: Suspended wheelset used for the dynamic analysis.

TABLE 2
The mechanical properties of the wheelset.

Description	Value
Mass	1568 kg
I_{xx}	656 kg.m^2
I_{yy}	168 kg.m^2
I_{zz}	656 kg.m^2
k_{l1}=k_{l2}	13,500 N/m
k_{t1}=k_{t2}	25,000 N/m
c_{l1}=c_{l2}	1000 N.s/m
c_{t1}=c_{t2}	0 N.s/m

mode shapes extracted from the modal analysis. The nodal displacement $\mathbf{U}$ and the nodal velocity vectors $\dot{\mathbf{U}}$ are calculated as follow:

$$\mathbf{U} = \mathbf{\Phi q} \tag{2.3}$$

$$\dot{\mathbf{U}} = \mathbf{\Phi \dot{q}} \tag{2.4}$$

where $\mathbf{\Phi}$ is the matrix of the mode shapes, $\mathbf{q}$ is the modal displacement vector and is $\dot{\mathbf{q}}$ the modal velocity vector.

Stresses can be reconstructed from the displacements as well, assuming that the damping moduli are known. In the case of stiffness-proportional damping for each material, the damping moduli $\boldsymbol{E}^v$ are proportional to the elastic moduli $\boldsymbol{E}$, with the same damping proportionality constant as the damping matrix. In other words, if the element damping matrix $\boldsymbol{c}^e = \alpha \boldsymbol{k}^e$, then $\boldsymbol{E}^v = \alpha \boldsymbol{E}$. The strain and strain rate can be recovered from the element nodal displacements and velocities in the standard manner, i.e.

$$\boldsymbol{\epsilon} = \boldsymbol{B}^e \boldsymbol{u}^e \tag{2.5}$$

$$\dot{\boldsymbol{\epsilon}} = \boldsymbol{B}^e \dot{\boldsymbol{u}}^e \tag{2.6}$$

where $\boldsymbol{B}^e$ is the standard finite element strain-displacement matrix. The stress, including the viscous component, can be written as

$$\boldsymbol{\sigma} = \boldsymbol{E}\boldsymbol{\epsilon} + \boldsymbol{E}^v \dot{\boldsymbol{\epsilon}} \tag{2.7}$$

3. Results

In this section, the main outputs of interest of the model are presented. We focus on the vertical displacements, the contact forces and the stresses. The bridge approach problem, as discussed above, is mainly the problem of settlement due to high stresses caused by a sudden change in stiffness in the supporting layer under the rail at the entrance and the exit of the bridge. We investigate a potential solution by placing a concrete slab under the ballast

layer that can rest on the edge of the abutment to minimise the settlement by decreasing the gradient of the stiffness variation.

Two designs of the slab are presented to investigate the effect of each of them: a rectangular slab and inclined slab. Figures (4a) and (4b) show the locations and the nodes numbers on the rail and soil where the vertical displacements are presented below.

The following figures compare different results for three cases: no slab, a rectangular slab in the approach zone, and an inclined slab in the approach zone.

In Figure (5), the vertical displacement at two general points away from the slab effect is presented. We can see in (5a) a rail point away before the slab area, while (5b) is a rail node in the middle of the bridge away after the slab. The figure shows nearly identical performance for the three cases at the two locations as predicted.

In Figure (6),the displacement of a node in the center of the slab is examined. Here, the effect of the slab in each of the three models is very clear. As anticipated, the highest value of vertical displacement is associated with the case of no slab, while it gets better with rectangular slab, 19% reduction in the vertical displacement, and the best result is the one of the inclined slab model, as it gradually increases the stiffness as the track approaches the bridge, leading to a nearly 52% reduction in the vertical displacement at that location.

In Figures (7-9) rail points at the bridge approach zone are presented. Figure (7) shows the vertical displacement of the rail node above the last sleeper before the abutment, while Figure (8) shows the vertical displacement for the last rail node before the abutment. Continuing on the track, Figure (9) shows the vertical displacement for the first rail node above the abutment.

These three figures show clearly the effect of the two slabs on the reduction of the vertical displacement of the rail, compared to the no-slab case. As shown in Figure (7), the rail node above the last sleeper before the abutment, the use of the rectangular slab and the inclined slab reduced the vertical displacement by about 44% and 71% respectively compared to the no-slab case.

In Figure (8), the last rail node before the abutment, the use of the rectangular slab and the inclined slab reduced the vertical displacement by about 46%

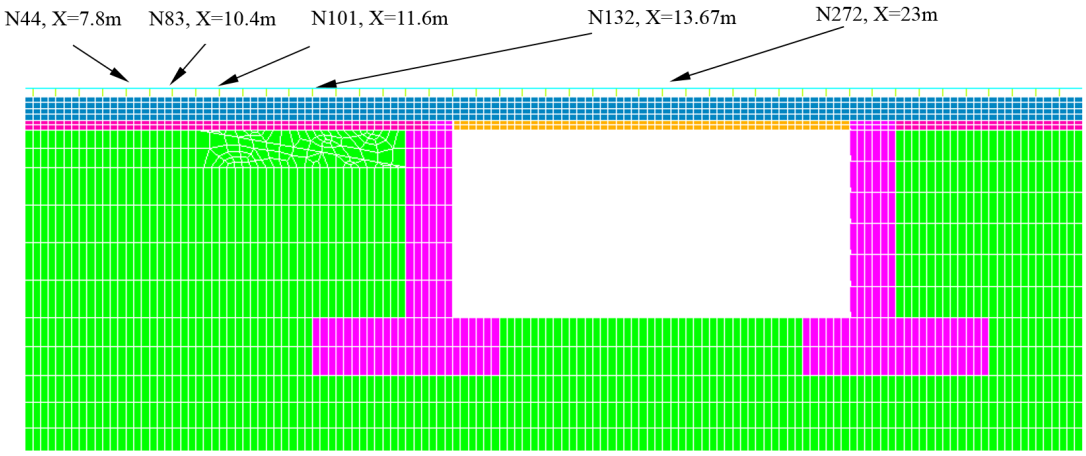

(a)

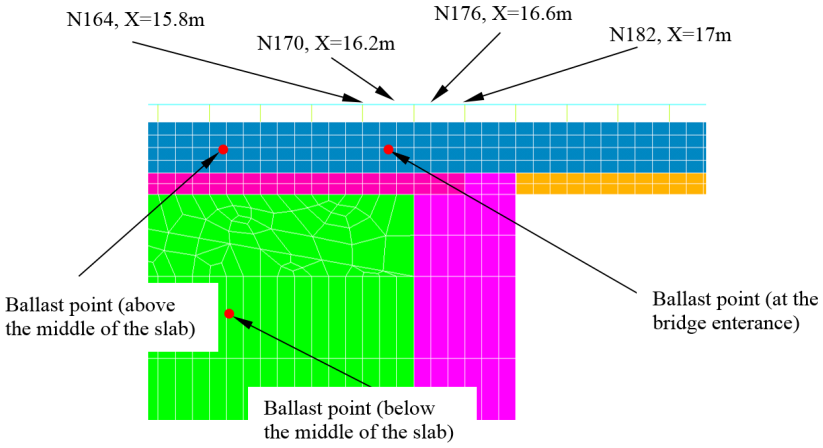

(b)

Fig 4: (a) Points of interests on the rail (b) Points on the approach and soils.

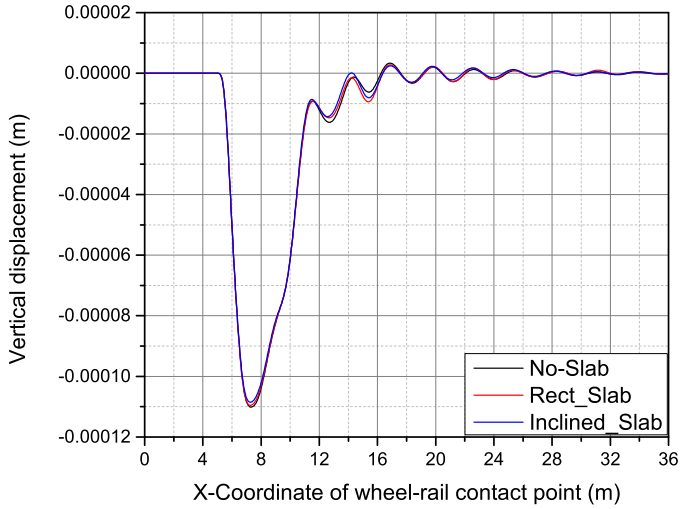

(a)

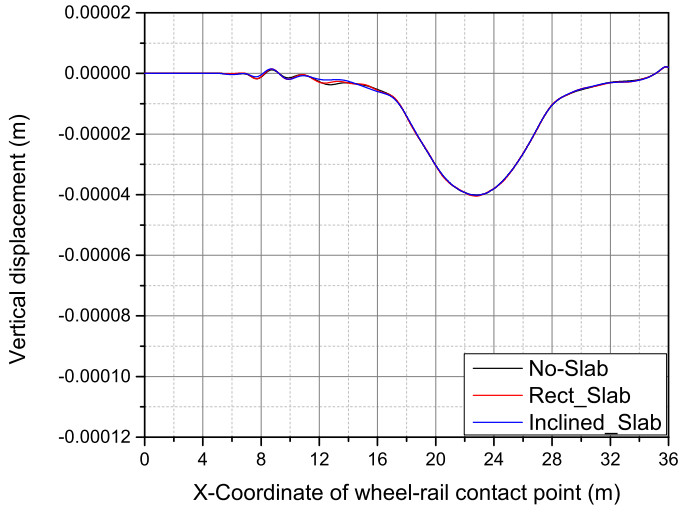

(b)

Fig 5: Vertical displacement away from the slab effect, (a) Node 44, a general rail point away before the slab effect (B) Node 272, a rail point in the middle of the bridge, see Figure 4a.

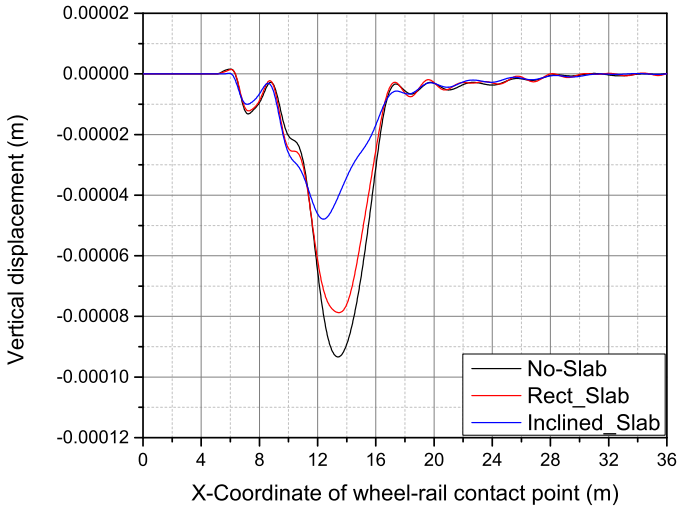

Fig 6: Vertical displacement of Node 132, a rail point above the slab middle point, see Figure 4a.

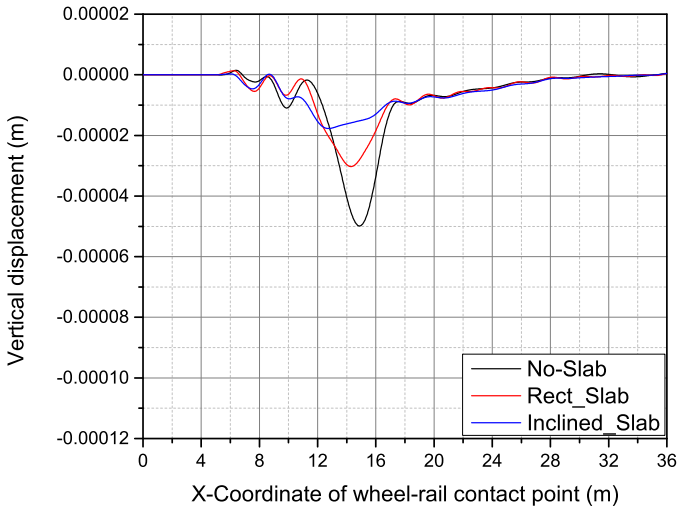

Fig 7: Vertical displacements of Node 164, a rail point on last sleeper before the abutment, see Figure 4b.

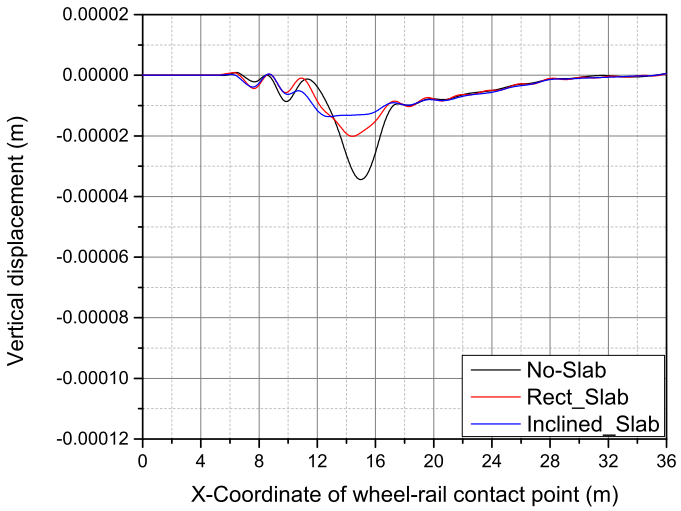

Fig 8: Vertical displacements of Node 170, the last rail node before the abutment, see Figure 4b.

and 68% respectively compared to the no-slab case. The same trend of reduction is also shown in Figure (9), the rail node above the first sleeper above the abutment, the use of the rectangular slab and the inclined slab reduced the vertical displacement by about 45% and 58% respectively compared to the no-slab case.

The above figures and the associated percentages in the vertical displacements reduction show the effectiveness of the implementation of both the rectangular and the inclined slabs in the bridge approach zone, especially the inclined slab, which has smaller displacments. By comparing the displacements between (7) and (9) which represents the last slab before the abutment and the first slab above the abutment respectively, we can see clearly how the slabs reduce the vertical "jump" in the rail displacement when the vehicle crosses the entrance of the bridge. In numbers, the no-slab case has 75% change in the height of the vertical displacement, and 60% in the rectangular slab case, while it is only 43% in the inclined slab case; however, we should pay attention to the absolute values before and after the abutment to recognise that the 43% is from a smaller vertical displacement

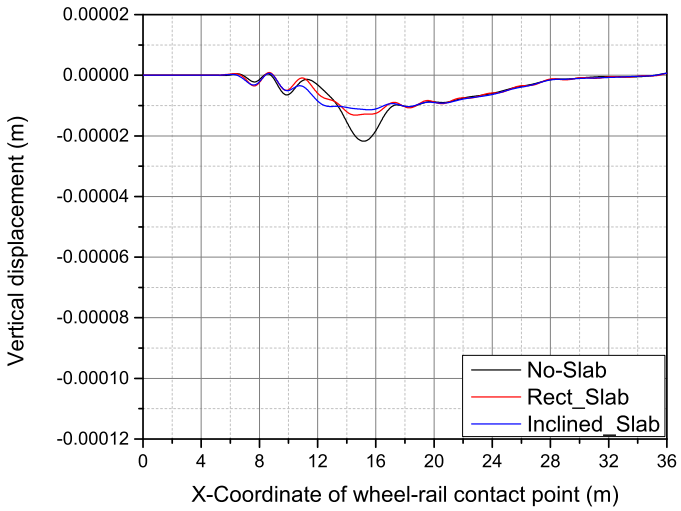

Fig 9: Vertical displacement of Node 176, the first rail point after the beginning of the abutment, see Figure 4b.

compared to the no slab case.

It is also important to mention here that the effect of the slabs starts from the beginning of the slab section, not only before the abutment at the bridge approach zone. As seen in Figure (10) the vertical displacement of the rail around the slab beginning is presented at two locations. Figure (10a) shows rail node above the last sleeper before the beginning of the slab, and we can see it shows already slight difference between the three cases due to the effect of the implemented slabs. While (10b) shows the vertical displacement of the rail node above the first sleeper on the slab, we can see clearly the effect of the different slab designs on the system performance via the variation in the displacement peak values even where the slab effect is just starting.

Besides the rail nodes, the results of a couple points in the ballast and subgrade are also shown. In Figure (11), the vertical displacement of a node in the ballast under the last sleeper before the abutment and a node on the subgrade under the last sleeper before the abutment are presented. As shown in (11a), the ballast node, the ballast vertical displacement is decreased with the use of the slabs, with a reduction of 33% for the rectangular slab and

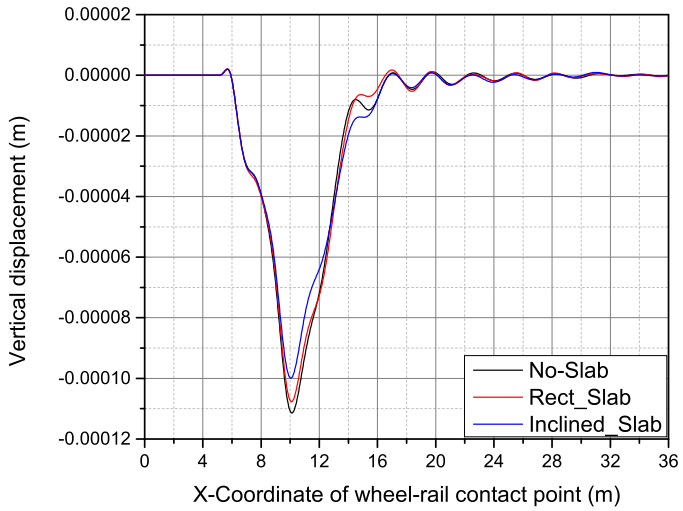

(a)

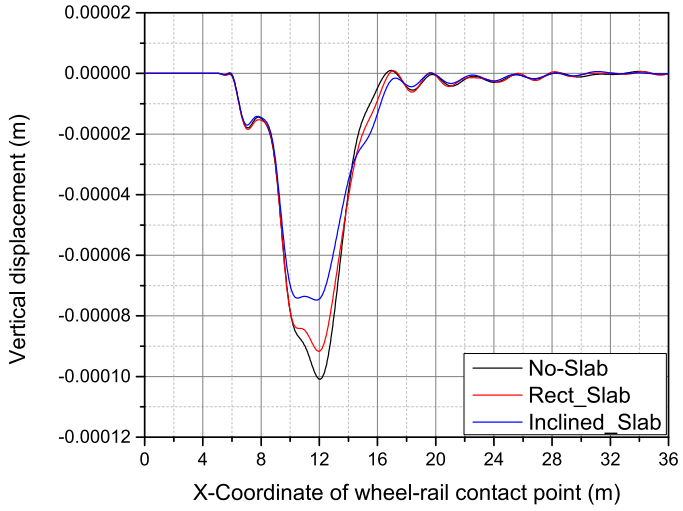

(b)

Fig 10: Vertical displacement away around the slab beginning, (a) Node 83, a rail point on last sleeper before the slab (B) Node 101, a rail point on first sleeper of the slab, see Figure 4a.

62% for the inclined slab. We can see similar behaviour in (11b), the subgrade node as well. The rectangular slab shows a reduction in the displacement of 33% while the inclined slab shows a reduction of about 40% compared to the case of no slab.

The wheel/rail contact force is also a significant factor to investigate in this study, as it is an indicator of ride quality and impact on the track structure. Figure (12) compares the contact force for the three models: no slab, rectangular slab, and inclined slab. As we can see in the figure, the model with no slab has the highest jump in the contact force value as the wheelset approaches the bridge entrance zone, while having a rectangular slab reduces the peak of the jump, while the case of inclined slab shows an even smoother variation in compared to the other cases. It is important to mention here that the magnitude of the force is speed dependent; however, the results show improved performance even with higher speed.

It is important to point out that using the slabs did not shift the jump in the contact force from the bridge entry to the beginning of the slab. The contact force for the three cases was found to be almost the same.

Besides the vertical displacement and forces, it is important to examine the stresses in the soil, knowing that high stresses can lead to settlement of the soil, exacerbating the issues associated with bridge approaches. The stress is compared for the three cases for both ballast and subgrade. the following figures show the change in the stress from the elastic stress caused by gravity, which means that the gravity effect was excluded for the three cases and hence why the graphs start at zero stress.

Figure (13) represents the stress in the substructure, the stress in the ballast above the middle of the slab is presented in (13a), while the stress in the subgrade below the middle point of the slab is presented in (13b). We can see that the slabs do not have a significant effect on the ballast stress at that point; however, the slabs reduce the stress in the subgrade at same location.

Another point of interest is the ballast performance just before the bridge entrance. The slab implementations, especially the inclined one, show improvement in the stress level at that critical point, as shown in Figure 14.

Figure 15 shows the vertical acceleration of the wheetset. Acceleration is related to occupant comfort on the train. Though the focus of this study is on the effects of the substructure stress which could cause settlement and

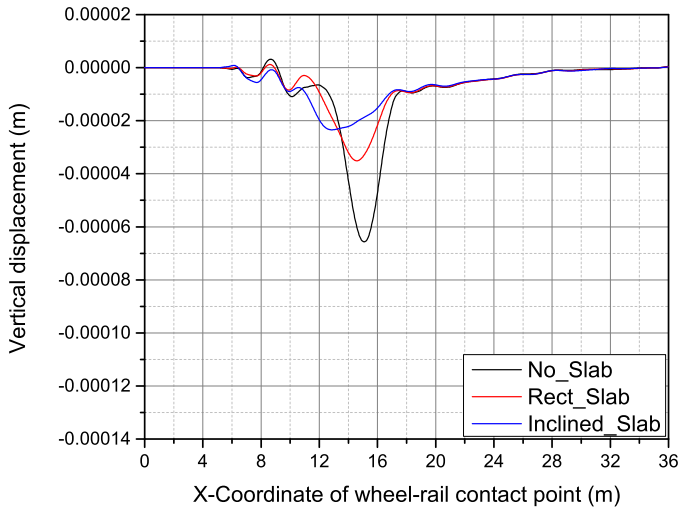

(a)

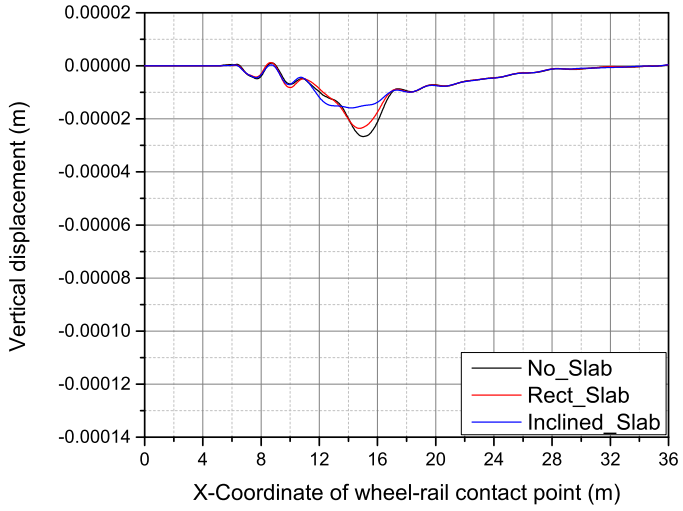

(b)

Fig 11: Vertical displacement away around the slab beginning, (a) Node 83, a rail point on last sleeper before the slab (B) Node 101, a rail point on first sleeper of the slab, see Figure 4b.

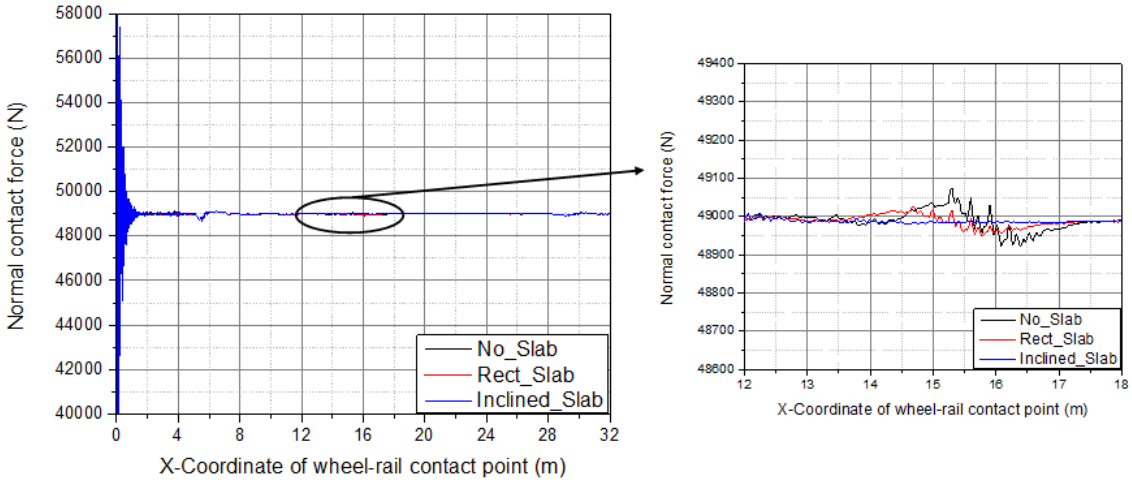

Fig 12: Wheel/rail contact force, the inset showing the the area near the bridge entrance.

the need for maintenance, we can see that slab, especially the inclined slab, reduced accelerations on the wheelset. Initially, there is significant vibration from the drop onto the rigid portion of the track and then the transition to the flexible portion. There is still some residual vibration at the start of the approach, but this vibration is damped out very quickly in the case of the inclined slab. The no slab case and to a lesser extent the rectangular slab has renewed vibration as the wheelset approaches the bridge.

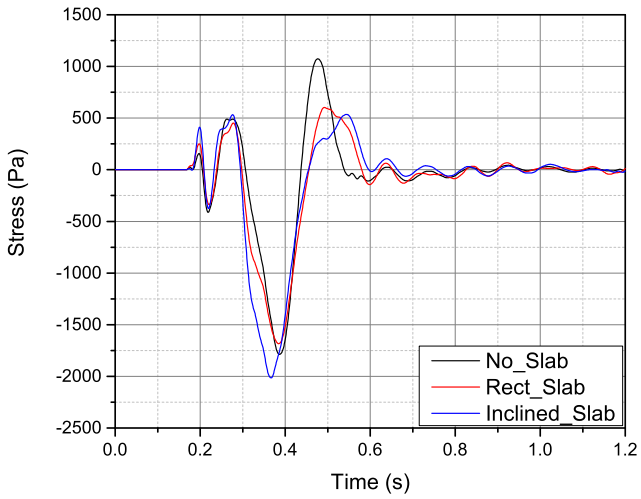

(a)

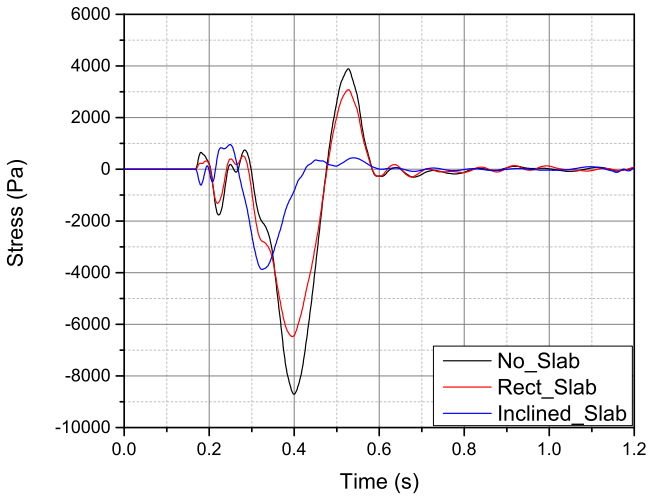

(b)

Fig 13: Difference in vertical stress from unloaded case in (a) the ballast above the middle of the slab, (b) the subgrade below the middle of the slab, see Figure 4a.

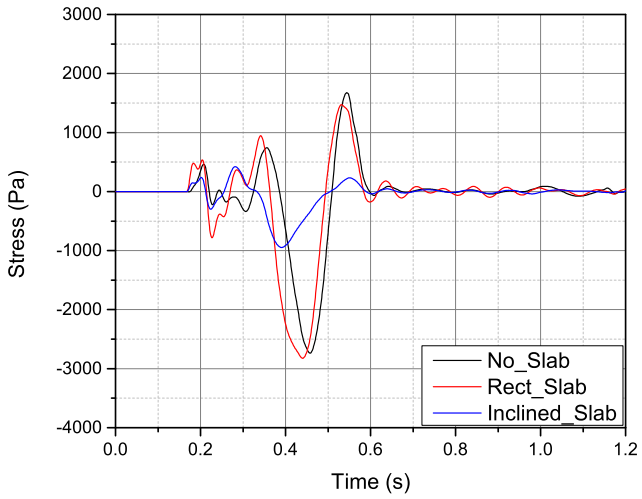

Fig 14: Difference in vertical stress from unloaded case in the ballast just before the bridge entrance, see Figure 4b.

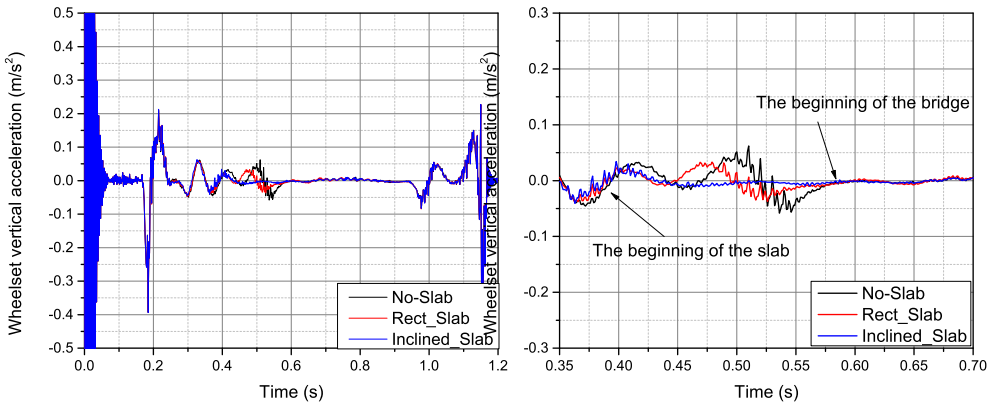

Fig 15: Vertical acceleration of the suspended wheelset in (left) the full simulation and (right) near the bridge approach.

4. Conclusions

The bridge approach problem is a common problem in the railroad industry. This problem exists due to the sudden stiffness change from the substructure before and after the bridge. This sudden stiffness change can cause large stresses, which can in turn lead to soil settlement, which leads to a change in the rail level. This rail change in level causes a sudden impact which develops high level of contact force, faster wear of rail surface, and discomfort for passengers.

A full 3D bridge model was built using FE and coupled with a MBS code using modal decomposition, which is based on selecting the most important mode shapes, and the nodal elimination, selecting the nodes under external forces, and provide the modal information of these selected nodes to the MBS code. The purpose of this model was to study the effectiveness of constructing a concrete slab below the ballast at the bridge approach zone. The slab creates a more gradual change in the stiffness, improving ride quality, lessening the wear in the wheel and the rail surface, and hence reducing the maintenance cost. We compare three cases: no slab, rectangular slab, and inclined slab. The rectangular slab has a constant thickness, while the inclined slab has a linearly increasing thickness to increase the stiffness from the soft soil to the stiff bridge.

The work investigated the model performance regarding the vertical displacement of the rail nodes as well as the soil nodes. The results show great improvement in the performance with both slabs, especially, as expected, with the inclined slab. The vertical displacements were reduced considerably at different locations and show smoother level of change from the soil to the bridge. The contact forces were investigated as well, and the results show a good reduction in the force peak at the entrance of the bridge when the slabs were used, and, again, the inclined slab showed better performance. The analysis also showed that the implementation of the slab did not simply move the force peak from the abutment to the beginning of the slab.

Another important factor to investigate in this study was the stress in the soil. High stresses can cause increase soil settlement and lead to degradation of the material. The implementation of slab has an effect on the performance of the soil, especially the subgrade. The stress figures show how the stress in the models with the implemented slabs have been reduced in the subgrade layer

below the slabs, which show the effectiveness of the presented methodology and also the effectiveness of the used slabs. The stress in the ballast was not affected greatly by the slab.

In general, the results discussed in this work show clearly the effectiveness of the coupling technique, presented in this work, between FEM and MBS codes. The model is created using FEM and then the main outputs of the modal analysis are provided to the MBS code, after nodal elimination. This approach can save significant amount of time and allows us to construct more complicated models with more details. The results also show the effectiveness of the slab implementation at the bridge entrance and how it has a clear effect on the displacements (for rails and soil), the wheel/rail contact force, and the stress level in the subgrade at the bridge approach zone.

In this work, we have verified a methodology for analysing a bridge approach problem and some potential solutions. With little modification, the coupled technique can be applied to an instrumented bridge site for validation, at least in the case with no slab. Field measurements to compare the model results with respect to the measured values as in the field measurement work done by Mishra et al. [29]. Here an entire train car model may be necessary to realistically capture pitch and other effects of an actual moving train. Hanging sleepers may also affect the behaviour as the ballast settles near the approach.

Acknowledgements

This project was supported by the National University Rail (NURail) Center - a US DOT OST-R University Transportation Center.

References

[1] Xiao XB, Wen ZF, Jin XS, and Sheng XZ. Effects of track support failures on dynamic response of high speed tracks. *International Journal of Nonlinear Sciences and Numerical Simulation*, 8(4):615–630, 2007.

[2] Xinbiao Xiao, Xuesong Jin, Yongquan Deng, and Zhongrong Zhou. Effect of curved track support failure on vehicle derailment. *Vehicle System Dynamics*, 46(11):1029–1059, 2008.

[3] H. Chebli, D. Clouteau, and L. Schmitt. Dynamic response of high-speed ballasted railway tracks: 3d periodic model and in situ measurements. *Soil Dynamics and Earthquake Engineering*, 28(2):118 – 131, 2008.

[4] G. Kumaran, Devdas Menon, and K. Krishnan Nair. Dynamic studies of railtrack sleepers in a track structure system. *Journal of Sound and Vibration*, 268(3):485 – 501, 2003.

[5] Mauri Koskinen. Modeling of soil-structure interaction between railway bridge and soil. In *ABAQUS Users' Conference*, 2005.

[6] E Tutumluer. *Discrete element modeling of railroad ballast settlement.* PhD thesis, University of Illinois, 2007.

[7] Y. S. Wu, Y. B. Yang, and J. D. Yau. Three-dimensional analysis of train-rail-bridge interaction problems. *Vehicle System Dynamics*, 36(1):1–35, 2001.

[8] Ahmed A. Shabana, Mahmoud Tobaa, Hiroyuki Sugiyama, and Khaled E. Zaazaa. On the computer formulations of the wheel/rail contact problem. *Nonlinear Dynamics*, 40(2):169–193.

[9] Ahmed A. Shabana and Jalil R. Sany. A survey of rail vehicle track simulations and flexible multibody dynamics. *Nonlinear Dynamics*, 26(2):179–212.

[10] P Galvín, A Romero, and J Domínguez. Fully three-dimensional analysis of high-speed train–track–soil-structure dynamic interaction. *Journal of Sound and Vibration*, 329(24):5147 – 5163, 2010.

[11] M Tanabe, H Wakui, M Sogabe, N Matsumoto, and Y Tanabe. A combined multibody and finite element approach for dynamic interaction analysis of high-speed train and railway structure including post-derailment behavior during an earthquake. *IOP Conference Series: Materials Science and Engineering*, 10(1):012144, 2010.

[12] Jorge Ambrósio, João Pombo, Frederico Rauter, and Manuel Pereira. *Multibody Dynamics: Computational Methods and Applications*, chapter A Memory Based Communication in the Co-simulation of Multibody and Finite Element Codes for Pantograph-Catenary Interaction Simulation, pages 231–252. Springer Netherlands, Dordrecht, 2009.

[13] Ahmed I El-Ghandour, Martin B Hamper, and Craig D Foster. Coupled finite element and multibody system dynamics modeling of a three-dimensional railroad system. *Proceedings of the Institution of Mechanical Engineers, Part F: Journal of Rail and Rapid Transit*, 230(1):283–294, January 2016.

[14] J. L. Briaud, R. W. James, and S. B Hoffman. *Settlement of Bridge Approaches:(the Bump at the End of the Bridge).*, volume 234. National Academy Press, 1997.

[15] G. Monley and J. Wu. Tensile reinforcement effects on bridge approach settlement. *Journal of Geotechnical Engineering*, 119(4):749–762, 1993.

[16] Sam M.B. Helwany, Jonathan T.H. Wu, and Burkhard Froessl. {GRS} bridge abutmentsan effective means to alleviate bridge approach settlement. *Geotextiles and Geomembranes*, 21(3):177 – 196, 2003.

[17] D. Li and D. Davis. Transition of railroad bridge approaches. *Journal of Geotechnical and Geoenvironmental Engineering*, 131(11):1392–1398, 2005.

[18] T Dahlberg. Railway track stiffness variations consequences and countermeasures. *International Journal of Civil Engineering*, 8(1):1–12, 2010.

[19] J. Zhang, J. J. Zheng, , and Y. Lu. Evaluation of the new technique of geogrid-reinforced and pile-supported embankment at bridge approach. *Journal of Bridge Engineering*, 19(4):06014001, 2014.

[20] Andre Paixao, Eduardo Fortunato, and Rui. Calada. Design and construction of backfills for railway track transition zones. *Proceedings of the Institution of Mechanical Engineers, Part F: Journal of Rail and Rapid Transit*, 2013.

[21] Jennifer Elizabeth. Nicks. *The bump at the end of the railway bridge.* PhD thesis, Texas A&M University, 2009.

[22] Edward J. Hoppe. Guidelines for the use, design, and construction of bridge approach slabs. *No. VTRC 00-R4*, 1999.

[23] Meli E and Pugi L. Preliminary development, simulation and validation of a weight in motion system for railway vehicles. *Meccanica*, 48(10):25412565., 2013.

[24] A. A. Shabana, K. E. Zaazaa, and H. Sugiyama. *Railroad vehicle dynamics: A computational approach*. Taylor & Francis CRC, Boca Raton, FL, 2007.

[25] Ahmed A. Shabana. *Dynamics of multibody systems*. Cambridge University Press, 2005.

[26] A A Shabana, R Chamorro, and C Rathod. A multi-body system approach for finite-element modelling of rail flexibility in railroad vehicle applications. *Proceedings of the Institution of Mechanical Engineers, Part K: Journal of Multi-body Dynamics*, 222(1):1–15, 2008.

[27] C Rathod, R Chamorro, J L Escalona, M El-Sibaie, and A A Shabana. Validation of three-dimensional multi-body system approach for modelling track flexibility. *Proceedings of the Institution of Mechanical Engineers, Part K: Journal of Multi-body Dynamics*, 223(4):269–282, 2009.

[28] Ahmed A. Shabana. *Computational Dynamics*. John Wiley & Sons, 2010.

[29] D. Mishra, E. Tutumluer, T. D. Stark, J. P. Hyslip, S. M. Chrismer, and M. Tomas. Investigation of differential movement at railroad bridge approaches through geotechnical instrumentation. *Journal of Zhejiang University SCIENCE A*, 13(11):814–824, 2012.